π^+p Interactions at 900 MeV*†

W. J. METZGER,‡ B. FORMAN, A. C. MELISSINOS, AND T. YAMANOUCHI
Department of Physics and Astronomy, University of Rochester, Rochester, New York
(Received 19 January 1967; revised manuscript received 23 June 1967)

We report the results of the investigation of 18 500 frames of π^+p interactions in the Brookhaven 20-in. bubble chamber at an incident energy of 900 MeV. It is found that single-pion production proceeds almost entirely through formation of the N_{33}^* isobar. The production mechanism of the N_{33}^* is analyzed in terms of its spin density matrix. Comparison is made with Stodolsky and Sakurai's ρ-exchange model and with the absorptive peripheral model.

I. INTRODUCTION

IN recent years, considerable effort has been devoted to investigation of the production of π mesons by pions on nucleons. The experiments of Stonehill,[1] Gensollen *et al.*,[2] Tautfest and Willman,[3] Foelshe and Kraybill,[4] and Kraybill *et al.*[5] concern π^+p interactions in the energy range from 0.5 to 1.4 BeV/c. In the present paper we report the results of the analysis of 5000 interactions of 900-MeV π^+ mesons on protons. These were obtained from an exposure in the BNL 20-in. liquid-hydrogen bubble chamber. The main contributing channels are elastic scattering and single-pion (mainly neutral) production:

$$\pi^+p \rightarrow \pi^+p\,, \tag{1}$$

$$\pi^+p \rightarrow \pi^+p\pi^0. \tag{2}$$

Whereas the main purpose of the experiment was to study the pion production mechanism, we also examined the possible existence of a $T=1$ dipion resonance in the region of 300- to 700-MeV invariant mass. Such a resonance, called the "ζ meson," had been previously reported[6,7] at a mass of 580 MeV. Since the ρ meson[8] is also a $T=1$ resonance decaying into two pions, the primary energy was chosen so as to minimize ρ production.

It was found that reaction (2) proceeds mainly through production of an N_{33}^* resonance in association with a pion

$$\pi^+p \rightarrow N^{*++}+\pi^0 \rightarrow \pi^+p\pi^0\,,$$
$$N^{*+} +\pi^+ \rightarrow \pi^0p\pi^+.$$

The above two channels account for 95% of the entire π^0 production process.

In Sec. III, the cross sections for the different partial channels are given and the elastic scattering data are analyzed. In Sec. IV the production of isobars is investigated, and it is shown that the data for reaction (2) are consistent with 95% isobar production. The usual analysis in terms of the spin density matrix[9] for a $J=\frac{3}{2}$ resonance is applied, and the matrix elements are determined. These results are not in good agreement with the predictions of the Stodolsky-Sakurai[10] model. In this model it is assumed that ρ exchange dominates the production mechanism which is then treated in analogy with electroproduction of isobars [see Fig. 8(a)]. This model has been fairly successful[11,12] in describing the similar reaction $K^+p \rightarrow K^0p\pi^+$. These results are also compared with calculations using the absorptive peripheral model,[13] where better agreement is found.

Finally in Sec. V some data on the other final states

* Work supported by the United States Atomic Energy Commission.

† Submitted by W. J. Metzger in partial fulfillment of the requirements for the Degree of Doctor of Philosophy at the University of Rochester.

‡ Present address: Brookhaven National Laboratory, Upton, New York.

[1] D. Stonehill *et al.*, Phys. Rev. Letters **6**, 624 (1961); D. Stonehill and H. Kraybill, Rev. Mod. Phys. **34**, 503 (1962).

[2] C. Gensollen, P. Granet, R. Barloutaud, A. Leveque, and J. Meyer, in *Proceedings of the Sienna International Conference on Elementary Particles and High-Energy Physics, 1963*, edited by G. Bernardini and G. P. Puppi (Societa Italiana di Fisica, Bologna, 1963), Vol. I, p. 84.

[3] G. W. Tautfest and R. B. Willman, in *Proceedings of the Second Topical Conference on Resonant Particles* (Ohio University, Athens, Ohio, 1965), p. 421.

[4] H. W. J. Foelshe and H. L. Kraybill, Phys. Rev. **134**, B1138 (1964).

[5] H. L. Kraybill, D. L. Stonehill, B. Deler, W. Laskar, J. P. Merlo, G. Valladas, and G. W. Tautfest, Phys. Rev. Letters **16**, 863 (1966).

[6] R. Berloutaud, J. Heughebaert, A. Leveque, J. Meyer, and R. Omnes, Phys. Rev. Letters **8**, 32 (1962).

[7] The possible existence of the ζ, on the evidence of the early experiments, has been discussed by M. Roos, Phys. Letters **3**, 242 (1963).

[8] See, for example, A. R. Erwin, R. March, W. D. Walker, and E. West, Phys. Rev. Letters **6**, 628 (1961); E. Pickup, D. K. Robinson, and E. O. Salant, *ibid.* **7**, 192 (1961); D. D. Carmony and R. T. Van de Walle, Phys. Rev. **127**, 456 (1960); D. L. Stonehill and H. L. Kraybill, Rev. Mod. Phys. **34**, 503 (1962).

[9] J. D. Jackson, Nuovo Cimento **34**, 1644 (1964); K. Gottfried and J. D. Jackson, *ibid.* **33**, 309 (1964).

[10] L. Stodolsky and J. Sakurai, Phys. Rev. Letters **11**, 90 (1963); L. Stodolsky, Phys. Rev. **134**, B1099 (1964).

[11] B. Kehoe, Phys. Rev. Letters **11**, 93 (1963).

[12] M. Ferro-Luzzi, R. George, Y. Goldschmidt-Clermont, V. P. Henri, B. Jongejans *et al.*, in *Proceedings of the Sienna International Conference on Elementary Particles and High-Energy Physics, 1963*, edited by G. Bernardini and G. P. Puppi (Societa Italiana di Fisica, Bologna, 1963), Vol. I, p. 189; G. R. Lynch, M. Ferro-Luzzi, R. George, Y. Goldschmidt-Clermont, V. P. Henri *et al.*, Phys. Letters **9**, 359 (1964); Aachen-Berlin-Birmingham-Bonn-Hamburg-London (I.C.)-München Collaboration, Phys. Letters **10**, 229 (1964); M. Abolins, D. D. Carmony, D.-N. Hoa, R. L. Lander, C. Rindfleisch, and N. Xuong, Phys. Rev. **136**, B195 (1964).

[13] J. D. Jackson and H. Pilkuhn, Nuovo Cimento **33**, 906 (1964); J. D. Jackson, J. T. Donohue, K. Gottfried, R. Keyser, and B. E. Y. Svensson, Phys. Rev. **139**, B428 (1965).

are presented; these data, however, do not show any prominent features.

II. EXPERIMENTAL PROCEDURE

The analysis was carried out on about 18 500 frames of π^+ mesons from separated beam[14] No. 1 at the Brookhaven AGS; on the average there were 15 tracks per frame. The mean beam momentum and dip angle were determined from distributions of the measured quantities for a large sample of events which had given successful kinematic fits. The mean momentum is 1.02 $\pm$0.06 BeV/c and the mean dip angle is $-0.5°\pm0.8°$. These values (rather than the measured values) were then used for all beam tracks in the kinematic fitting.

Because of the measured efficiency of the beam separators, beam contamination by protons is believed to be negligible. The μ^+ contamination is estimated to be $(9\pm3)\%$. The chamber operating conditions were such that a minimum ionizing track would produce about 12 bubbles/cm. Adequate visual estimates of ionization in the range of one to three times minimum could then be made.

From a second scan of a portion of the film, the overall scanning efficiency was found to be $(94\pm3)\%$. The number of beam tracks in every tenth frame was counted by the scanners. All two-pronged and four-pronged events within a fiducial volume approximately 28 cm in length along the beam were measured with precision measuring machines. Usually five or six points were measured on each track in each of the two views which were most favorable for stereo reconstruction.

The measurements were input to the Brookhaven National Laboratory programs TRED and KICK for reconstruction and kinematic fitting. Events rejected by TRED or which gave no vertex fits in KICK were remeasured. Both kinematic fitting and estimates of bubble density were used for all events in order to identify the final state. An event which fitted a four-constraint (4C) interpretation was identified as such, provided that the bubble density of all tracks was consistent with the interpretation. An event which was not consistent with a four-constraint interpretation but which made a one-constraint (1C) fit was accepted as such, provided that the bubble density of all tracks was consistent with the interpretation.

Events which gave only fits which were inconsistent with the observed bubble density or which gave more than one fit which was consistent with bubble density were remeasured in the hope that a second measurement would resolve the ambiguity. If the second remeasurement did not produce a unique acceptable fit, the event was called ambiguous and was not processed further. Events which, for both measurements, could not be reconstructed were also called ambiguous. Ambiguous events were not processed further and were for the purpose of cross sections distributed proportionately among the other categories. Events which for both measurements could not be fitted were assumed to be events with more than one missing neutral.

In Figs. 1(a) and (b), we show the distributions of the square of the missing mass for elastic and $\pi^+p\pi^0$ events, respectively. It is seen that the resolution is of the order of $\sigma=0.001$ and $\sigma=0.012$ BeV^2, respectively, allowing good separation of these two classes of events. Also in Figs. 2(a) and (b) are given the χ^2 distributions for the 4C and 1C events. The solid curves are the theoretical distributions multiplied by a stretch factor of $\alpha^2=0.7$ for both cases and with the addition of a constant background as indicated in the figures.

Some difficulty arose in connection with elastic events having slow protons, since these can usually be fitted[15] by the hypothesis $\pi^+\pi^+n$. A small fraction of such events that did not fit the 4C hypothesis (presumably because of large measurement errors) were tested for coplanarity, $\cos\varphi$, and for the effective mass of the pion-neutron system. On the basis of these two criteria, namely, that $-1<\cos\varphi<-0.985$ and $M(\pi^+n)<1170$ MeV, 53 $\pi^+\pi^+n$ events were reclassified as elastics.

III. CROSS SECTIONS

The number of events found within the fiducial volume for each final state are given in column (2) of Table I. It is necessary to apply corrections for:

(a) Missed small-angle elastic scattering events. There is a bias against events having steep, short protons. An angle φ is defined by $\cos\varphi=\hat{c}\cdot\hat{n}$, where $\hat{n}$ is the unit vector normal to the scattering plane and $\hat{c}$ is a unit vector along the camera axis. Events should be distributed isotropically in φ. Figure 3 shows the distributions in φ (folded about 90°) and the corrections for various intervals in $\cos\theta_\pi$, the center-of-mass pion scattering angle. No corrections were needed for $\cos\theta<0.7$. The total correction was 97 ± 21 events. In addition, the distribution of $\cos\theta_\pi$ (which peaks forward) shows a lack of events in the region $\cos\theta\geq0.9$. This region was corrected by extrapolating a third-order polynomial fit in $\cos\theta_\pi$ (see Fig. 4). This led to a further correction of 232 ± 15 in the total number of elastic events.

(b) Identification biases. The squares of the missing mass for the elastic and the $\pi^+p(\pi^0)$ events have been shown in Fig. 1 and are distributed as expected, indicating that no corrections are needed. The correction for elastic events misidentified as $\pi^+\pi^+n$ events has been described in Sec. II above.

(c) Muon contamination of the beam which requires an increase of $(9\pm3)\%$ in all cross sections.

(d) A correction of $(6\pm3)\%$ for scanning efficiency.

The yields in each channel after application of the above corrections are given in column (3) of Table I.

[14] C. Baltay *et al.*, Nucl. Instr. Methods **20**, 37 (1965).

[15] For more details see W. J. Metzger, thesis, University of Rochester, 1966 (unpublished).

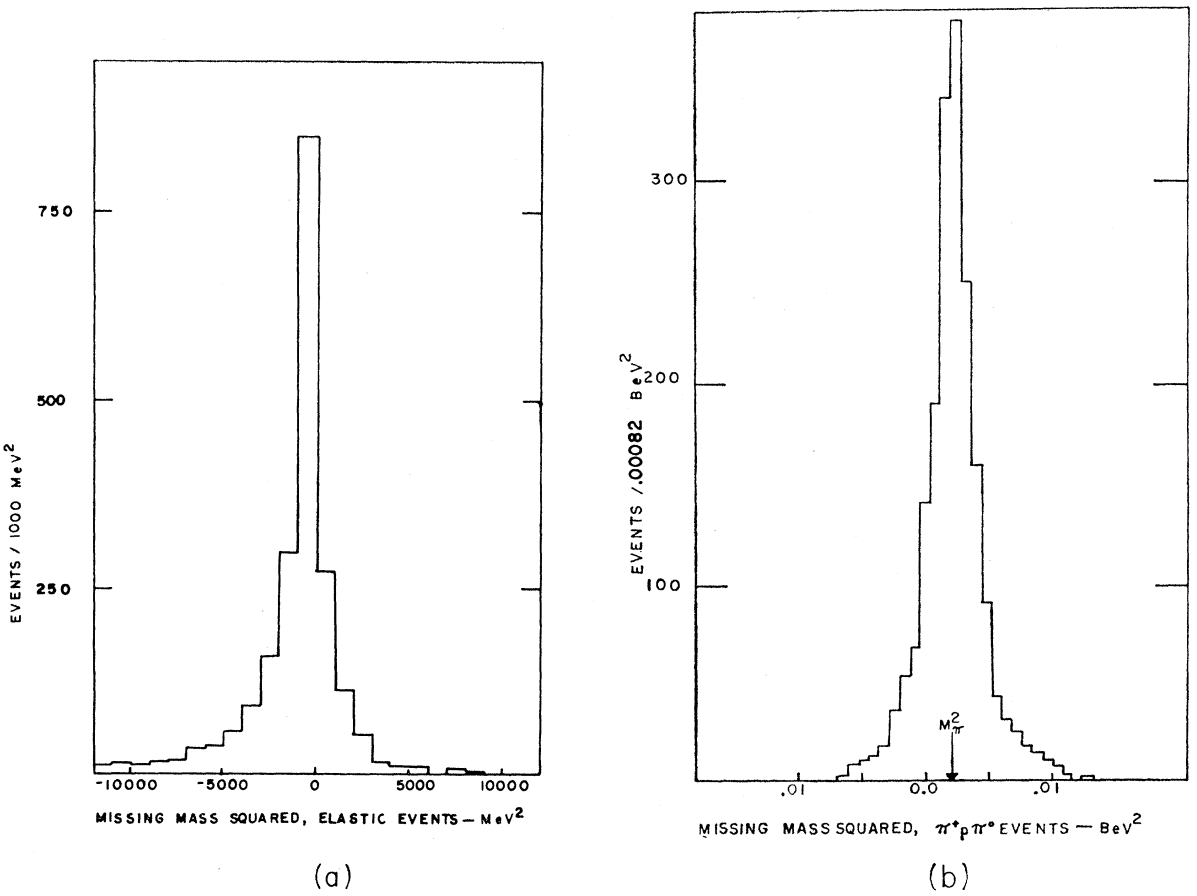

FIG. 1. Distribution of missing-mass squared. (a) Events accepted as elastic; (b) events accepted as single π^0 production events.

The cross sections are calculated as

$$\sigma = NW/L\rho N_A n,$$

where N is the number of interactions, W is the gram molecular weight of H_2, L is the total beam track length, ρ is the density of liquid hydrogen, taken as 0.062 g/cm³, N_A is Avogadro's number, and n is the number of atoms per molecule of H_2. The length within the fiducial volume of each track is 28±0.3 cm, and the total track length is (8.05±0.10)×10⁶ cm.

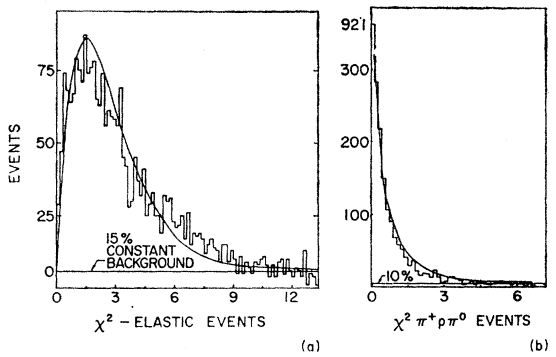

FIG. 2. χ^2 distribution. (a) All elastic events; (b) all $\pi^+p\pi^0$ events.

Since the total number of interactions within the fidicial volume (after corrections) is 6552±257 events, this leads to a total cross section of 22.0±0.9 mb. This is consistent with the more accurate counter data of Brisson *et al.*[16] which gives 23.2±0.7 mb. We have therefore normalized our total cross section to this value and obtain the partial cross sections given in column (4) of Table I.

TABLE I. π^+p cross sections at 1.02 BeV/c.

Final state	Number of events in the fiducial volume: Actual	Corrected	Cross section (mb)
π^+p	2060±45	3135±132	11.10±0.47
$\pi^+p\pi^0$	1955±44	2509±105	8.88±0.37
$\pi^+\pi^+n$	411±22	528± 33	1.87±0.12
$\pi^+pe^+e^-\gamma$	27±11	31± 12	0.11±0.04
2-prongs (≥2 neutrals)	158±18	202± 22	0.72±0.08
4-prongs (not incl. Dalitz pairs)	127±20	146± 24	0.52±0.08
Unidentified or ambiguous 2-prongs	577±24		
Total	5315±76	6552±257	23.2

[16] J. C. Brisson *et al.*, Nuovo Cimento **19**, 210 (1961).

The elastic differential cross section is shown in Fig. 4 and in Table II, together with the results of a least-squares fit of the form

$$\frac{d\sigma}{d\Omega}=\sum_{n=0}^{N}\alpha_n\cos^n\theta.$$

The lowest-order fit which is satisfactory (low enough χ^2) is a third-order ($N=3$) polynomial. For 34 degrees of freedom, the value of χ^2 is 36.6. Higher-order fits are not significantly better. The coefficients α_n, given below, are in agreement with the results of others[2,17,18]:

$$\alpha_0=0.26\pm0.02 \text{ mb/sr},$$
$$\alpha_1=0.65\pm0.06 \text{ mb/sr},$$
$$\alpha_2=1.80\pm0.08 \text{ mb/sr},$$
$$\alpha_3=1.02\pm0.13 \text{ mb/sr}.$$

TABLE II. Elastic differential cross section.

$\cos\theta_\pi$	Number of events Actual	Number of events Corrected for folded φ	Cross section (mb/sr) From data	Cross section (mb/sr) From 3rd-order polynomial fit
0.975	55	66.6±11.0	0.97±0.16[a]	3.55±0.15
0.925	137	163.5±15.6	2.39±0.23[a]	3.20±0.14
0.875	162	184.5±16.7	2.69±0.24	2.89±0.11
0.825	170	190.5±17.0	2.78±0.25	2.59±0.09
0.775	139	147.4±12.8	2.15±0.19	2.32±0.08
0.725	141	148.5±12.9	2.17±0.19	2.06±0.06
0.675	119	119 ±10.9	1.74±0.16	1.83±0.05
0.625	113	113 ±10.6	1.65±0.15	1.61±0.05
0.575	82	82 ± 9.1	1.20±0.13	1.42±0.04
0.525	101	101 ±10.0	1.47±0.15	1.24±0.04
0.475	83	83 ± 9.1	1.21±0.13	1.08±0.03
0.425	80	80 ± 8.9	1.17±0.13	0.94±0.03
0.375	66	66 ± 8.1	0.96±0.12	0.81±0.03
0.325	47	47 ± 6.9	0.69±0.10	0.69±0.03
0.275	40	40 ± 6.3	0.58±0.09	0.59±0.03
0.225	32	32 ± 5.7	0.47±0.08	0.51±0.02
0.175	29	29 ± 5.4	0.42±0.08	0.43±0.02
0.125	19	19 ± 4.4	0.28±0.06	0.37±0.02
0.075	22	22 ± 4.7	0.32±0.07	0.32±0.02
0.025	21	21 ± 4.6	0.31±0.07	0.27±0.02
−0.025	13	13 ± 3.6	0.19±0.05	0.24±0.02
−0.075	13	13 ± 3.6	0.19±0.05	0.22±0.02
−0.125	11	11 ± 3.3	0.16±0.05	0.20±0.02
−0.175	14	14 ± 3.7	0.20±0.05	0.19±0.02
−0.225	20	20 ± 4.5	0.29±0.07	0.19±0.02
−0.275	16	16 ± 4.0	0.23±0.06	0.19±0.02
−0.325	13	13 ± 3.6	0.19±0.05	0.20±0.02
−0.375	18	18 ± 4.2	0.26±0.06	0.21±0.02
−0.425	20	20 ± 4.5	0.29±0.07	0.23±0.02
−0.475	19	19 ± 4.4	0.27±0.06	0.25±0.02
−0.525	17	17 ± 4.1	0.25±0.06	0.27±0.02
−0.575	29	29 ± 5.4	0.42±0.08	0.29±0.02
−0.625	20	20 ± 4.5	0.29±0.07	0.31±0.02
−0.675	13	13 ± 3.6	0.19±0.05	0.33±0.02
−0.725	32	32 ± 5.7	0.47±0.08	0.35±0.02
−0.775	25	25 ± 5.0	0.36±0.07	0.37±0.02
−0.825	22	22 ± 4.7	0.32±0.07	0.38±0.03
−0.875	27	27 ± 5.2	0.39±0.08	0.39±0.03
−0.925	29	29 ± 5.4	0.42±0.08	0.40±0.04
−0.975	31	31 ± 5.6	0.45±0.08	0.40±0.05

[a] These points are unphysically low because they have not been corrected for small-angle scanning loss. They were not used in the fit.

[17] F. Grard *et al.*, Nuovo Cimento **22**, 193 (1961).
[18] J. A. Helland *et al.*, Phys. Rev. **134**, B1062 (1964).

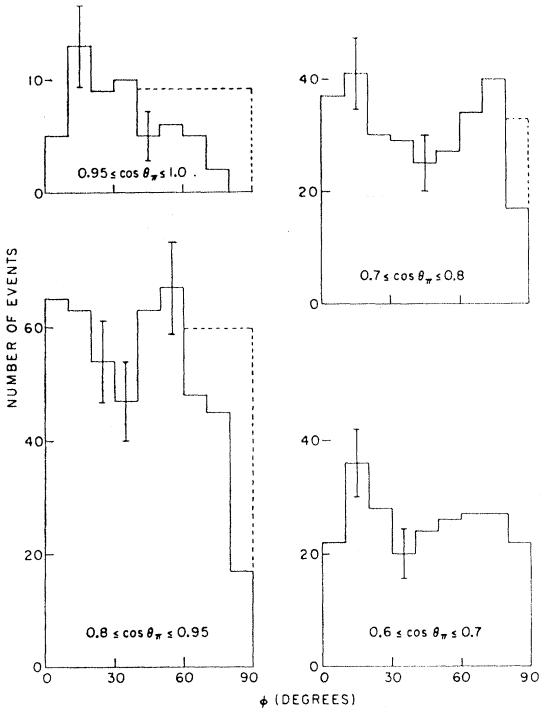

FIG. 3. Distribution of φ (folded) for various intervals in $\cos\theta_\pi$. The dashed line shows the corrections made.

IV. $\pi^+p\pi^0$ FINAL STATE

A. Cross Sections for Resonance Production

Figure 5(a) shows a Dalitz plot for the $\pi^+p\pi^0$ final state. The N_{33}^{*++} and N_{33}^{*+} isobars appear as bands centered at approximately 1.5 BeV² in the π^+p and π^0p effective-mass squared, respectively, indicating predominance of the $N_{33}^{*++}\pi^0$ and $N_{33}^{*+}\pi^+$ final state.

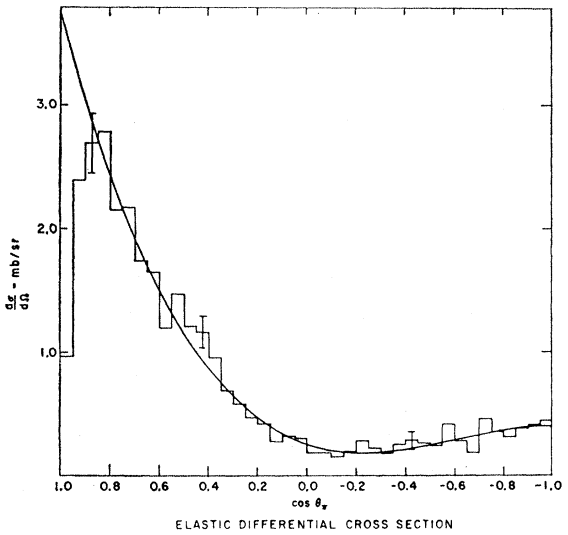

FIG. 4. Elastic differential cross section. The curve shown is a third-order polynomial fit to the data (see text).

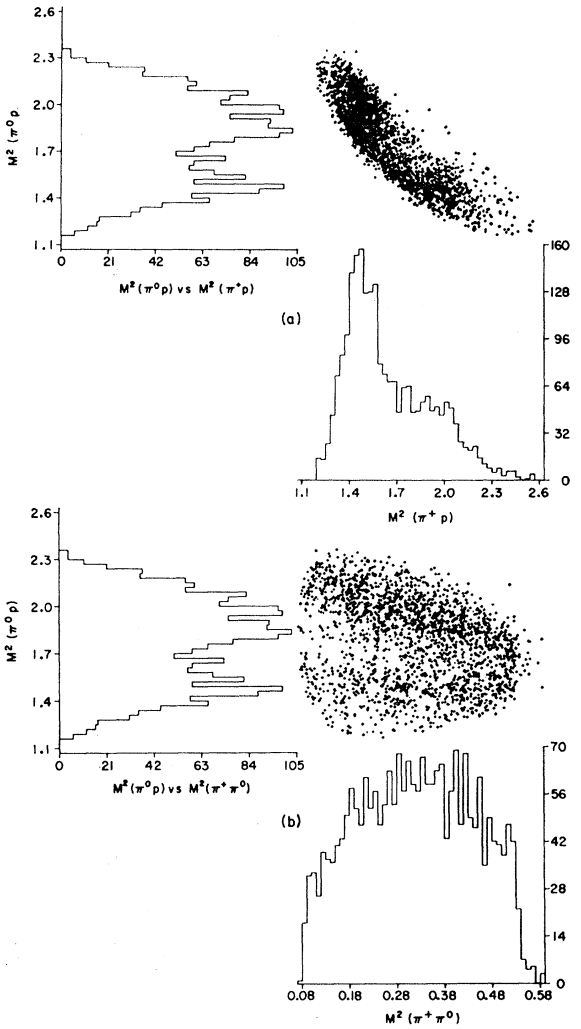

FIG. 5. Dalitz plots of the square of the $\pi^0 p$ invariant mass versus (a) that of the $\pi^+ p$, and (b) that of the $\pi^+\pi^0$, in BeV².

Note that the broad peak in the $p\pi^0$ mass plot at approximately 1.9 BeV² is a kinematical "reflection" of N_{33}^{*++} production. Figure 5(b) shows again the Dalitz plot for this final state but now in terms of $p\pi^0$ and $\pi^+\pi^0$ effective-masses squared.

In order to determine cross sections for the production of such quasi-two-body final states, the three mass spectra were fitted, ignoring possible interference between resonances, with a sum of Lorentz-invariant phase space[19] and a term for each resonance. This resonance term was invariant phase space weighted by a simple Breit-Wigner resonance formula, $\alpha/[(M-M_0)^2+(\frac{1}{2}\Gamma)^2]$. The only parameters varied in the fitting were the amount of each resonance, α_i. The masses and widths were fixed at the values shown in Table III. The values for the N_{33}^* were chosen to coincide with the position and width of the experimental peaks. These values differ from those for the actual mass and width because the N_{33}^* is a p-wave resonance and hence has an energy-dependent width.[9]

TABLE III. Parameters used in fitting the mass spectra and the resulting cross sections.

Quasi-two-body final state	Resonance parameters: Mass (MeV)	Full width (MeV)	Fitted cross section[a]: (% of $\pi^+p\pi^0$ final state)	(mb)
$N^{*++}(1236)+\pi^0$	1220	90	$62.7_{-2.9}^{+2.8}$	$5.57_{-0.26}^{+0.25}$
$N^{*+}(1236)+\pi^+$	1220	90	$27.7_{-2.8}^{+2.5}$	$2.46_{-0.26}^{+0.23}$
$N^{*+}(1518)+\pi^+$	1518	120	$0.0_{-0.0}^{+1.0}$	$0.00_{-0.00}^{+0.09}$
$\rho^+ + p$	763	106	$4.4_{-4.4}^{+4.1}$	$0.39_{-0.39}^{+0.36}$
Nonresonant phase space			$5.2_{-5.2}^{+6.8}$	$0.46_{-0.46}^{+0.60}$

[a] The errors are 95% confidence limits (see text).

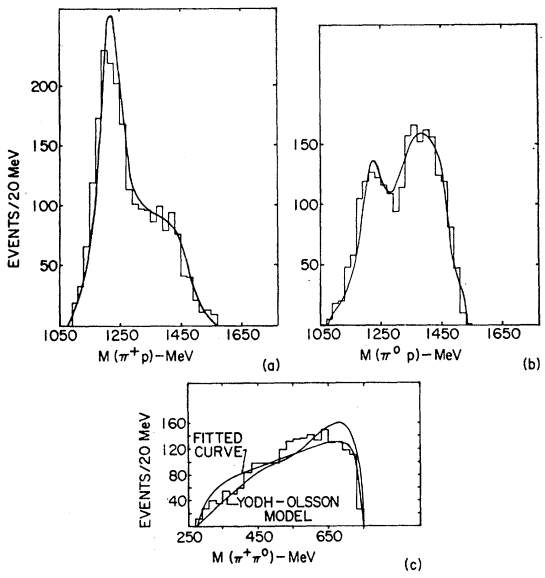

FIG. 6. Distribution of (a) the $\pi^+ p$ invariant mass; (b) the $\pi^0 p$ invariant mass; (c) the $\pi^+\pi^0$ invariant mass. The curves are fitted superpositions of phase space and resonance Breit-Wigner forms. In (c) is also shown the prediction of the Yodh-Olsson model.

All three mass histograms were fitted *simultaneously* using the maximum-likelihood method[20] as described in the Appendix. The fit consisted in finding the relative amount of quasi-two-body final states and pure phase space that maximize the likelihood function (minimize the χ^2). The results (in %) are shown in column (4) of Table III, and the fitted mass spectra in Figs. 6(a), 6(b), and 6(c).

From Table III, we note that the production of the state $[N^{*+}(1518)+\pi^+]$ is consistent with zero. Simi-

[19] The Lorentz-invariant phase space for a three-particle final state is given by

$$F(P,m_1,m_2,m_3)=\int[\prod_{i=1}^{3} d^4p_i\delta(p_i^2-m_i^2)]\delta^4(\sum_{j=1}^{3} p_j-P),$$

where m_i are the rest masses of the three final-state particles and p_i their four-momenta; P is the total four-momentum.

[20] H. Cramer, *Mathematical Methods of Statistics* (Princeton University Press, Princeton, 1964).

larly, the contribution of $[\rho^++p]$ and of the nonresonant phase space are both minimal (if not zero). We therefore conclude that at 900-MeV incident energy the reaction $\pi^+p\rightarrow p\pi^+\pi^0$ is consistent with *pure* $N^*(1236)$ production. We also note that the ratio

$$\frac{\sigma[N^{*++}(1236)+\pi^0]}{\sigma[N^{*+}(1236)+\pi^+]}=2.26\pm0.23,$$

as required from isospin invariance which predicts for this ratio 2.25.

To obtain quantitative confidence limits on our above conclusions, we make use of the fact[20,21] that if

$$\lambda(\alpha_i)=\frac{\mathfrak{L}(\alpha_1^*,\alpha_2^*,\cdots\alpha_i,\cdots\alpha_k^*)}{\mathfrak{L}(\alpha_1^*,\alpha_2^*,\cdots\alpha_i^*,\cdots\alpha_k^*)},$$

then $I=-2\ln\lambda$ is distributed as χ^2 with k degrees of freedom. As explained in the Appendix, $\mathfrak{L}(\alpha_1^*,\alpha_2^*,\cdots\alpha_k^*)$ is the likelihood function evaluated at the best estimators α_i^*.

It is important to note that k is the number of parameters fitted (k is *not* the number of bins, n, which gives the degrees of freedom for the χ^2 of the fit proper). In the present case, we have only three parameters, namely, α_1, the amount of $[N^{*++}(1236)+\pi^0]$ [note that this fixes the amount of $[N^{*+}(1236)+\pi^+]$]; α_2, the amount of $[\rho^++p]$; and α_3, the amount of nonresonant phase space; but we have only two free parameters, because of the normalization condition

$$\sum_{i=1}^{3}\alpha_i=1.$$

Thus the value of $I=-2\ln\lambda=6.0$ corresponds to 95% confidence limits; these are given in Table III.

A problem of considerable interest is the (electromagnetic) mass differences between the various charge states of the N_{33}^* isobar. These are difficult to determine experimentally because of the large width of the N_{33}^* and of the appearance of interference effects. Furthermore, from Fig. 6 we immediately note that the backgrounds for the N^{*++} and N^{*+} are completely different.

Nevertheless, we have attempted to fit the data of Fig. 6 with a p-wave resonance of the form[22]

$$\sigma(\omega)\propto\omega_0^2\Gamma^2(\omega)/[(\omega_0-\omega)^4+\omega_0^2\Gamma^2(\omega)],$$

with

$$\Gamma(\omega)=\Gamma_0(q/q_0)^3[\rho(\omega)/\rho(\omega_0)],$$

where $\rho(\omega)=(am_\pi^2+q^2)^{-1}$ and $a=1.3$ for m_π and q in MeV; q is the momentum of the decay products in the N^* rest frame where the width parameter Γ_0 was fixed at 120 MeV and the ratio $N^{*++}/N^{*+}=2.25$. Similarly the ratio of N^* production to nonresonant phase space

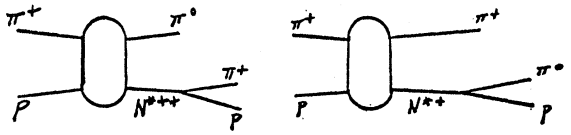

FIG. 7. The two possible diagrams for π^0 production via N^*.

was taken as 0.95/0.05. The positions of both N^{*++} and N^{*+} were varied, and the best fit for the π^+p and π^0p mass spectra *combined* gave $\chi^2=205$ for 45 degrees of freedom. The corresponding mass values are

$$M(N^{*++})=1229\pm6\text{ MeV},$$
$$M(N^{*+})=1229\pm3\text{ MeV}.$$

The above N^* masses still differ significantly from the known value of the isobar[23] at 1236 MeV and perhaps reflect the difficulty of obtaining a good mass value from this particular reaction.

B. $N_{33}^{*++}(1236)$

In view of the strong dominance of $N^*(1236)$ production, the Yodh-Olsson isobar model[24] may be applied. It incorporates p-wave decay of the $N^*(1236)$, but isobar production is still assumed isotropic (which is not in agreement with the data; see Fig. 9). The model assumes that the entire reaction proceeds via the two diagrams shown in Fig. 7 and takes into account the interference term and the requirement of Bose statistics.

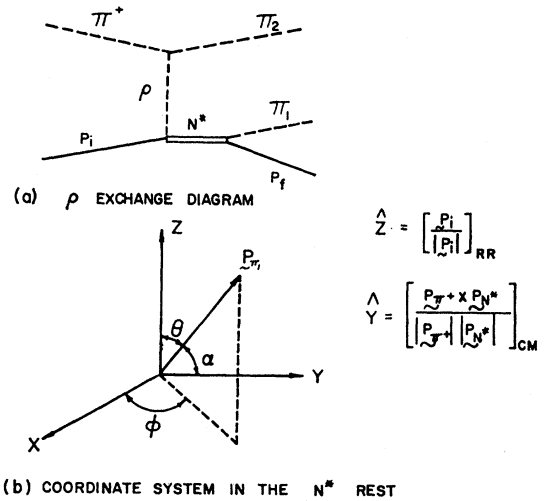

FIG. 8. (a) Feynman diagram for ρ-meson exchange. (b) Coordinate system in the N^* rest frame.

[21] S. S. Wilks, Annals of Mathematical Statistics 9, 60 (1938); M. S. Bartlett, Biometrika 40, 306 (1953).
[22] G. Gidal, A. Kernan, and S. Kim, Phys. Rev. 141, 1261 (1966).
[23] A. H. Rosenfeld *et al.*, Rev. Mod. Phys. 39, 1 (1967).
[24] M. Olsson and G. B. Yodh, Phys. Rev. Letters 10, 353 (1963); M. Olsson and G. B. Yodh, University of Maryland Technical Report No. 358, 1964 (unpublished); M. Olsson, University of Maryland Technical Report No. 379, 1964 (unpublished); M. G. Olsson and G. B. Yodh, Phys. Rev. 145, 1309 (1966).

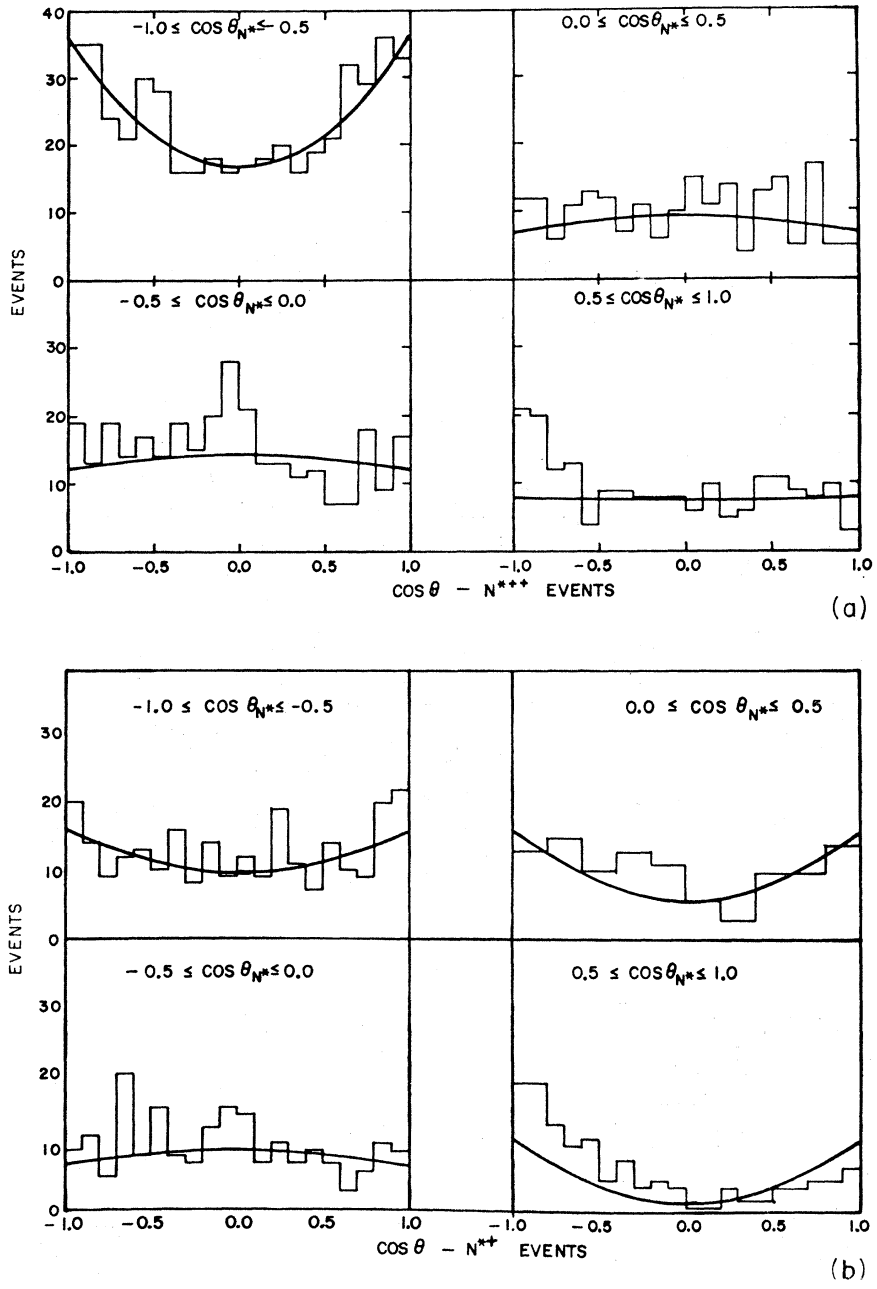

FIG. 9. Distributions of $\cos\theta$ for the following four intervals of the production angle:

$$-1.0 \leq \cos\theta_{N^*} \leq -0.5,$$
$$-0.5 \leq \cos\theta_{N^*} \leq 0.0,$$
$$0.0 \leq \cos\theta_{N^*} \leq 0.5,$$

and

$$0.5 \leq \cos\theta_{N^*} \leq 1.0$$

for (a) the N^{*++} events, and (b) the N^{*+} events.

The distribution predicted by this model for the $\pi^+\pi^0$ invariant mass (as given in Ref. 2) is included in Fig. 6(c) and shows good agreement with the data. Also the prediction of the Yodh-Olsson model for the branching ratio $\sigma(\pi^+p \to \pi^+p\pi^0)/\sigma(\pi^+p \to \pi^+\pi^+n)$, which is 5.0, is in very good agreement with our experimental result (see Table III) which is 4.8 ± 0.5. The simple isobar model of Lindenbaum and Sternheimer[25] predicts for this ratio 6.5.

Previous experiments at higher energy indicate that N^{*++} production in $\pi^+p \to \pi^0N^{*++}$ takes place largely via the ρ-exchange diagram [Fig. 8(a)]. For a one-meson-exchange diagram to apply to this reaction, the exchanged meson must have $I \geq 1$ in order to conserve isospin at the baryon vertex and $G=+1$ in order to conserve G parity at the meson vertex. The only known meson satisfying these criteria is the ρ meson. Similarly, the only meson exchange allowed for $K^+p \to K^0N^{*++}$ is the ρ. This reaction also has been found to proceed

[25] S. J. Lindenbaum and R. M. Sternheimer, Phys. Rev. **105**, 1874 (1957); S. J. Lindenbaum and R. M. Sternheimer, *ibid.* **106**, 1107 (1957); R. M. Sternheimer and S. J. Lindenbaum, Phys. Rev. **109**, 1723 (1958); S. Bergia, F. Bonsignori, and A. Stanghellini, Nuovo Cimento **15**, 1073 (1960).

largely by ρ exchange (both at 900 MeV [11] and at 3 GeV/c [12]). In particular, the ρ-exchange model of Stodolsky and Sakurai[10] has had a certain amount of success in predicting the decay angular distributions of the N^{*++} in these reactions. More recently, the absorptive peripheral model[13] has had a large degree of success in describing a wide variety of quasi-two-body reactions.

In order to investigate such exchange models, we select events as being N^{*++} or N^{*+} production if the π^+p or π^0p invariant mass is in the interval 1160–1280 MeV. In the rest frame of the N^*, the coordinate system shown in Fig. 8(b) is used.[9] The z axis is taken in the direction of the target proton and the y axis as normal to the production plane. The angle of the decay pion to the z axis is θ, and φ is its azimuthal angle. The angle φ is the Treiman-Yang angle,[26] as was shown by Jackson.[9] These angles are defined by the familiar relations

$$\cos\theta=(\mathbf{p}_t\cdot\mathbf{p}_1)/|(\mathbf{p}_t\cdot\mathbf{p}_1)|_{RR},$$

$$\cos\varphi=[(\mathbf{p}_b\times\mathbf{p}_r)\cdot(\mathbf{p}_1\times\mathbf{p}_2)]/|(\mathbf{p}_b\times\mathbf{p}_r)||(\mathbf{p}_1\times\mathbf{p}_2)|_{lab},$$

where $\mathbf{p}_b$ is the momentum of the beam, $\mathbf{p}_t$ is the momentum of the target proton, $\mathbf{p}_r$ is the momentum of the resonance, and $\mathbf{p}_1$ and $\mathbf{p}_2$ are the momenta of the two decay particles of the resonance, and where RR means evaluated in the rest frame of the resonance and lab means evaluated in the laboratory frame.

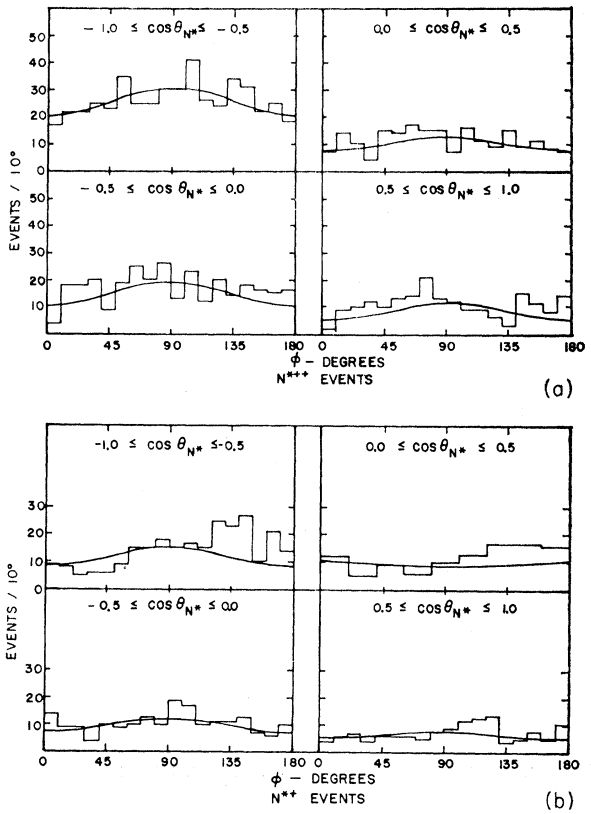

FIG. 10. Distributions of φ (the Treiman-Yang angle), for the same four intervals of the production angle as in the previous figure, for (a) the N^{*++} events, and (b) the N^{*+} events.

[26] S. B. Treiman and C. N. Yang, Phys. Rev. Letters 8, 140 (1962).

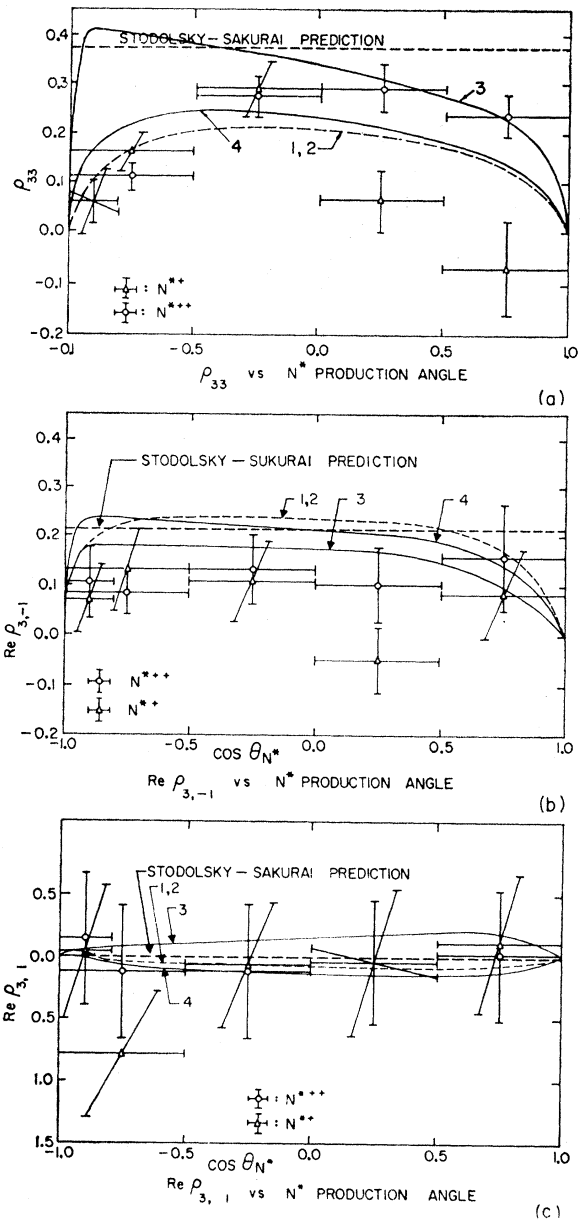

FIG. 11. The spin density matrix elements for the N^* versus the N^* production angle for (a) ρ_{33}, (b) Re$\rho_{3,-1}$, and (c) Re$\rho_{3,1}$. The values predicted by the Stodolsky-Sakurai model are shown (S-S). The results of the absorptive peripheral model calculations are shown for the following sets of coupling constants and absorption parameters:

(1) $G_1=G_2$, $G_3=0$, $C_1=C_2=1$, $\gamma_1=\gamma_2=0.5$;
(2) $G_1=G_2$, $G_3=0$, $C_1=C_2=1$, $\gamma_1=\gamma_2=0.3$;
(3) $G_1=G_2$, $G_3=0$, $C_1=C_2=0$, i.e., no absorption; and
(4) $G_2=1.14G_1$, $G_3=2G_1$, $C_1=C_2=1$, $\gamma_1=\gamma_2=0.5$.

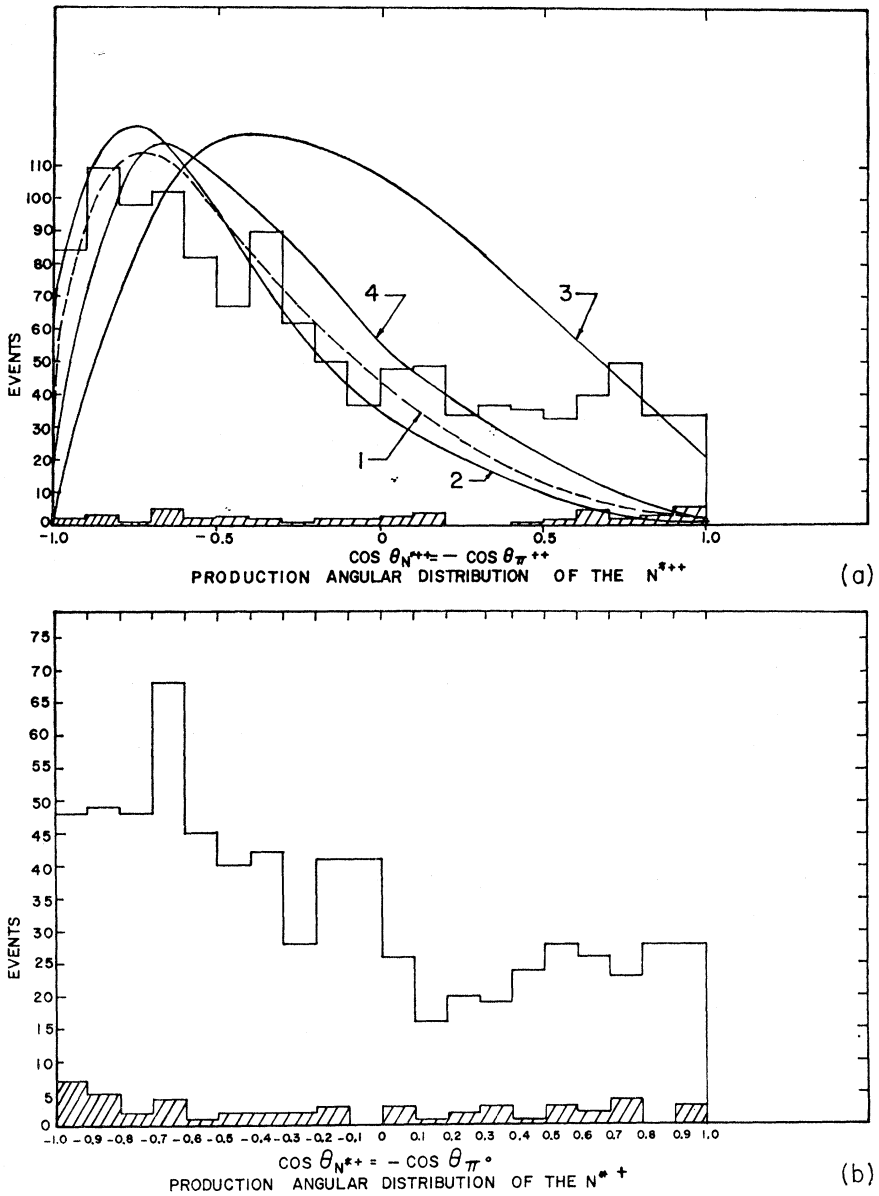

FIG. 12. Center-of-mass production angular distribution of isobars in the $\pi^+p\pi^0$ final state for (a) the N^{*++} and (b) the N^{*+}. The cross-hatched regions correspond to those events which are in both N^* bands. The results of the absorptive peripheral model calculation for the N^{*++} are shown. The curves are labeled the same as in Fig. 11.

The decay distribution $W(\theta,\varphi)$ for a spin-$\frac{3}{2}$ resonance is given[27] as

$$W(\theta,\varphi)=(3/4\pi)[\rho_{33}\sin^2\theta+\rho_{11}(\tfrac{1}{3}+\cos^2\theta)-(2/\sqrt{3})\,\mathrm{Re}\rho_{3,-1}\sin^2\theta\cos2\varphi-(2/\sqrt{3})\,\mathrm{Re}\rho_{3,1}\sin2\theta\cos\varphi],$$

where the $\rho_{mm'}$'s are the elements of the spin density matrix connecting the states m and m'; m and m' being twice the magnetic quantum numbers. Parity conservation in the production process requires that $\rho_{-m,-m'}=(-1)^{m-m'}\rho_{mm'}$. This in conjunction with the requirement that trace $\rho=1$ implies that $\rho_{33}=\frac{1}{2}-\rho_{11}$.

Integrating $W(\theta,\varphi)$ over θ and φ separately yields the following distributions:

$$W(\theta)\propto 1+4\rho_{33}+3(1-4\rho_{33})\cos^2\theta,$$

$$W(\varphi)\propto 1-(4/\sqrt{3})\,\mathrm{Re}\rho_{3,-1}\cos2\varphi$$

$$\propto 1+\frac{8\,\mathrm{Re}\rho_{3,-1}}{\sqrt{3}-4\,\mathrm{Re}\rho_{3,-1}}\sin^2\varphi.$$

Also, averaging $\sin2\theta\cos\varphi$ over the entire distribution yields

$$\mathrm{Re}\rho_{3,1}=-\tfrac{5}{8}\sqrt{3}\langle\sin2\theta\cos\varphi\rangle.$$

The density matrix elements, ρ_{11}, ρ_{33}, $\mathrm{Re}\rho_{3,-1}$, and $\mathrm{Re}\rho_{3,1}$, may therefore be determined from the distributions of $\cos\theta$ and φ and from the average value of

[27] J. D. Jackson, Rev. Mod. Phys. 37, 484 (1965); see also Ref. 9.

TABLE IV. N^* helicity density matrix elements.

Production angle interval (deg)	Isobar	Fit	χ^2	Number of degrees of freedom	Density matrix element
−1.0, −0.8	N^{*++}	$1+(1.85\pm0.70)\cos^2\theta$	14.7	18	$\rho_{33}=0.059\pm0.045$
		$1+(0.660\pm0.364)\sin^2\varphi$	13.8	16	$\mathrm{Re}\rho_{3,-1}=0.107\pm0.074$
		$\langle\sin2\theta\cos\varphi\rangle=-0.139\pm0.518$			$\mathrm{Re}\rho_{3,1}=0.15\pm0.56$
	N^{*+}	$1+(1.90\pm1.13)\cos^2\theta$	19.1	8	$\rho_{33}=0.056\pm0.070$
		$1+(0.412\pm0.545)\sin^2\varphi$	33.9	16	$\mathrm{Re}\rho_{3,-1}=0.074\pm0.115$
		$\langle\sin2\theta\cos\varphi\rangle=-0.039\pm0.531$			$\mathrm{Re}\rho_{3,1}=0.04\pm0.57$
−1.0, −0.5	N^{*++}	$1+(1.17\pm0.33)\cos^2\theta$	11.4	18	$\rho_{33}=0.110\pm0.028$
		$1+(0.492\pm0.205)\sin^2\varphi$	12.8	16	$\mathrm{Re}\rho_{3,-1}=0.085\pm0.043$
		$\langle\sin2\theta\cos\varphi\rangle=-0.110\pm0.513$			$\mathrm{Re}\rho_{3,1}=-0.119\pm0.555$
	N^{*+}	$1+(0.657\pm0.369)\cos^2\theta$	20.6	18	$\rho_{33}=0.160\pm0.041$
		$1+(0.876\pm0.430)\sin^2\varphi$	46.6	16	$\mathrm{Re}\rho_{3,-1}=0.132\pm0.084$
		$\langle\sin2\theta\cos\varphi\rangle=-0.073\pm0.475$			$\mathrm{Re}\rho_{3,1}=-0.79\pm0.514$
−0.5, 0.0	N^{*++}	$1+(-0.160\pm0.222)\cos^2\theta$	34.4	18	$\rho_{33}=0.278\pm0.041$
		$1+(0.895\pm0.356)\sin^2\varphi$	37.9	16	$\mathrm{Re}\rho_{3,-1}=0.134\pm0.070$
		$\langle\sin2\theta\cos\varphi\rangle=-0.092\pm0.461$			$\mathrm{Re}\rho_{3,1}=-0.110\pm0.551$
	N^{*+}	$1+(-0.244\pm0.287)\cos^2\theta$	30.1	18	$\rho_{33}=0.294\pm0.057$
		$1+(0.669\pm0.409)\sin^2\varphi$	17.5	16	$\mathrm{Re}\rho_{3,-1}=0.108\pm0.083$
		$\langle\sin2\theta\cos\varphi\rangle=-0.065\pm0.473$			$\mathrm{Re}\rho_{3,1}=-0.070\pm0.510$
0.0, 0.5	N^{*++}	$1+(-0.260\pm0.255)\cos^2\theta$	33.7	18	$\rho_{33}=0.297\pm0.051$
		$1+(0.624\pm0.370)\sin^2\varphi$	22.6	16	$\mathrm{Re}\rho_{3,-1}=0.103\pm0.076$
		$\langle\sin2\theta\cos\varphi\rangle=-0.032\pm0.501$			$\mathrm{Re}\rho_{3,1}=-0.035\pm0.502$
	N^{*+}	$1+(1.74\pm0.96)\cos^2\theta$	11.9	8	$\rho_{33}=0.067\pm0.064$
		$1+(-0.202\pm0.310)\sin^2\varphi$	16.2	7	$\mathrm{Re}\rho_{3,-1}=-0.049\pm0.066$
		$\langle\sin2\theta\cos\varphi\rangle=-0.038\pm0.556$			$\mathrm{Re}\rho_{3,1}=-0.041\pm0.599$
0.5, 1.0	N^{*++}	$1+(0.032\pm0.264)\cos^2\theta$	35.1	18	$\rho_{33}=0.245\pm0.043$
		$1+(1.17\pm0.58)\sin^2\varphi$	41.2	16	$\mathrm{Re}\rho_{3,-1}=0.160\pm0.109$
		$\langle\sin2\theta\cos\varphi\rangle=0.018\pm0.530$			$\mathrm{Re}\rho_{3,1}=0.019\pm0.529$
	N^{*+}	$1+(5.12\pm2.47)\cos^2\theta$	35.1	18	$\rho_{33}=-0.065\pm0.096$
		$1+(0.490\pm0.430)\sin^2\varphi$	16.9	16	$\mathrm{Re}\rho_{3,-1}=0.085\pm0.090$
		$\langle\sin2\theta\cos\varphi\rangle=0.109\pm0.518$			$\mathrm{Re}\rho_{3,1}=0.118\pm0.561$

$\sin2\theta\cos\varphi$. The density matrix elements $\rho_{3,-3}$ and $\rho_{1,-1}$, which are purely imaginary, and $\mathrm{Im}\rho_{3,-1}$ and $\mathrm{Im}\rho_{3,1}$ do not enter the decay distributions.

To determine the density matrix elements, we plot the experimental distributions of $\cos\theta$ and φ for various intervals of momentum transfer. These distributions are shown in Figs. 9(a) and (b) and 10(a) and (b) for the following angular intervals of N^* production: $-1\leqslant\cos\theta_{N^*}\leqslant-0.5$, $-0.5\leqslant\cos\theta_{N^*}\leqslant0.0$, $0.0\leqslant\cos\theta_{N^*}\leqslant0.5$, and $0.5\leqslant\cos\theta_{N^*}\leqslant1.0$. These limiting values of $\cos\theta_{N^*}$ correspond to Δ^2 values of 0.005, 0.214, 0.422, 0.631, and 0.839 $(\mathrm{BeV}/c)^2$ for an N^* mass of 1236 MeV. The solid lines on the figures are least-squares fits to the forms $A+B\cos^2\theta$ and $C+D\sin^2\varphi$, respectively.

From the above distributions and from the average value of $\sin2\theta\cos\varphi$, we obtain the matrix elements. These are listed in Table IV, which includes also other details of the fit. In the table we also give results for the interval $-1.0\leq\cos\theta_{N^*}\leq-0.8$, which corresponds to $\Delta^2\leq0.089$ $(\mathrm{BeV}/c)^2$; this is the region where we expect the best agreement between the data and the predictions of peripheral models.

We may compare our results with the model of Stodolsky and Sakurai,[10] which treats the ρ exchange in analogy to a one-photon exchange in electroproduction. They predict the following values for the density matrix elements: $\rho_{3,3}=\frac{3}{8}$, $\mathrm{Re}\rho_{3,-1}=\frac{1}{8}\sqrt{3}$, and $\mathrm{Re}\rho_{3,1}=0$. These matrix elements obviously lead to the angular distributions, $W(\theta)\propto1-\frac{3}{5}\cos^2\theta$ and $W(\varphi)\propto1+2\sin^2\varphi$. We note that the same distributions are arrived at[28] in the static model by Hara and in a quark model by Friar and Trefil.

In Figs. 11(a), (b), and (c) we have plotted the experimental values of the matrix elements given in Table IV and also show the predictions of the Stodolsky-Sakurai model. Whereas the agreement for $\rho_{3,1}$ is quite good for all Δ^2, in the case of $\rho_{3,-1}$ it is only fair, and for ρ_{33} the agreement is poor even for the smallest Δ^2. These results as well as a study of the distributions proper and of the (so-called Stodolsky-Sakurai) angle[29] α, lead us to the conclusion that this model cannot explain our data. A similar conclusion was reached by Tautfest and Willman[3] for incoming π^+ momenta of 1.11 and 1.265 BeV/c.

We have also attempted to fit our data using the

[28] Y. Hara, Phys. Rev. **140**, B1170 (1965); J. L. Friar and J. S. Trefil, CERN Report, 1966 (unpublished).

[29] The angle α is defined by

$$\cos\alpha=\{[\mathbf{p}_b\times(\mathbf{p}_1+\mathbf{p}_2)]_c\cdot(\mathbf{p}_1)_{RR}\}/[|\mathbf{p}_b\times(\mathbf{p}_1+\mathbf{p}_2)|_c|\mathbf{p}_1|_{RR}],$$

where the notation is the same as before; c means evaluated in the center-of-mass system. The angle α is not independent of θ and φ.

absorptive peripheral model of Jackson and collaborators,[13] even though its applicability at so low an energy is questionable. Calculations have been performed[30] for two sets of $N\rho N^*$ coupling constants[31]: (a) $G_1=G_2$ and $G_3=0$; and (b) $G_2=[2m_{N^*}/(m_p+m_{N^*})]G_1=1.14\,G_1$ and $G_3=2G_1$. In the nonrelativistic limit the first choice represents magnetic dipole absorption of the ρ, as in the Stodolsky-Sakurai model, but in general it also contains a small admixture of electric quadrupole absorption. This was the standard choice of Jackson and Pilkuhn.[13] The second choice is pure magnetic dipole. Results for three sets of absorption parameters[32] are included here: (a) no absorption, $C_1=C_2=0$; (b) $C_1=C_2=1$, $\gamma_1=\gamma_2=0.5$; and (c) $C_1=C_2=1$, $\gamma_1=\gamma_2=0.3$. The latter two choices are plausible, based on the elastic scattering data around 1 GeV/c, although it is rather unreasonable to assume purely diffractive, non-spin-flip scattering at this momentum.

For the same absorption parameters, the two choices of coupling constants give rather similar results. For this reason we show the results for only one of the sets of absorption parameters for the second choice of coupling constants. The results are shown in Fig. 12(a) for the differential cross section of the N^{*++}. The cross-section curves have been arbitrarily normalized to the data. We note that the shape of the curves with absorption is fairly similar to that of the data, especially for $\cos\theta<0$. The difference for $\cos\theta>0$ is very reasonable considering the dangers of applying the model at so low an incident momentum. The differential cross section of the N^{*+} [Fig. 12(b)] is similar to that of the N^{*++} for $\cos\theta<0$ but contains more events for $\cos\theta>0$. In Fig. 11 we show the results of the calculation for the density matrix elements together with the predictions

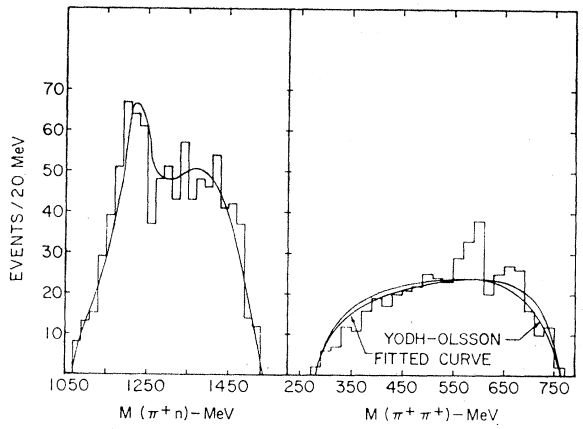

FIG. 13. Distributions of (a) the π^+n invariant mass and (b) the $\pi^+\pi^+$ invariant mass. The curves are a fitted superpositon of phase space and a Breit-Wigner resonance for the N^{*+} and the prediction of the Yodh-Olsson isobar model.

of the Stodolsky-Sakurai model as discussed above. We note that for $\cos\theta<-0.5$ the calculated values of ρ_{33} with absorption are reasonably close to experiment, and over the whole angular range are considerably better than the Stodolsky-Sakurai value. $\mathrm{Re}\rho_{3,-1}$ is rather insensitive to the presence of absorption; calculated values are similar to the Stodolsky-Sakurai values, in some disagreement with the data. All results for $\mathrm{Re}\rho_{3,1}$ are small in agreement with the data; but this is no test of the model.

Some time ago a dipion resonance called the ζ meson, of mass 580 MeV and narrow width, was reported by some experimenters[6,7]; observed in the $\pi^+\pi^0$ and $\pi^-\pi^0$ states but not in $\pi^+\pi^+$ or $\pi^-\pi^-$ states, it presumably had $T=1$. By inspecting the invariant mass spectrum of the $\pi^+\pi^0$ system given in Fig. 6(c), we see no evidence for such a narrow peak. The same conclusion can be reached when the data of Stonehill[1] ($T_\pi=910$ MeV) and of Barloutaud[2] ($T_\pi=900$ MeV) are combined with our data. We have also examined the $\pi^+\pi^0$ system after removing events in the "isobar bands" [$1160\leq M(\pi^+p)\leq 1280$ MeV or $1160\leq M(\pi^0p)\leq 1280$ MeV] but fail to see the ζ.

V. OTHER FINAL STATES

As can be seen from Table I, a significant number of 2-pronged events were found to be in the $\pi^+\pi^+n$ final state. These were treated in analogy to the $\pi^+p\pi^0$ state by forming the invariant-mass spectrum of the π^+n and $\pi^+\pi^+$ systems as shown in Fig. 13.

These spectra were fitted by an N^{*+} Breit-Wigner shape for pion number one, an N^{*+} Breit-Wigner shape for pion number two, and nonresonant phase space. Since pion number one and pion number two cannot be distinguished, the invariant mass of each is included in the same histogram. The constraint is imposed that the amount of N^* involving π_1 equal the amount involving π_2, which along with the constraint of normalization makes this a one-parameter fit.

The best fit gave a χ^2 of 130 for 45 degrees of freedom and is shown in Fig. 13, which also includes the Yodh-Olsson curve.[33] As a result of the fit we obtain

$$\begin{aligned}\sigma(\pi^+p\to\pi^+N^{*+}\to\pi^+\pi^+n)&=(55_{-10}^{+14})\%\text{ of }\sigma(n^+p\to\pi^+\pi^+n)\\&=1.05_{-0.19}^{+0.27}\text{ mb.}\end{aligned}\quad(1)$$

The errors are 95% confidence limits.

From Table III, we have the following cross sections:

$$\sigma(\pi^+p\to\pi^0N^{*++}\to\pi^+p\pi^0)=5.57_{-0.26}^{+0.25}\text{ mb},\quad(2)$$

$$\sigma(\pi^+p\to\pi^+N^{*+}\to\pi^+p\pi^0)=2.46_{-0.26}^{+0.23}\text{ mb},\quad(3)$$

the ratio of which agreed very well with that predicted by isospin invariance, namely 2.25 to 1. Isospin in-

[30] J. D. Jackson (private communication).
[31] The coupling constants are defined in J. D. Jackson and H. Pilkuhn, Nuovo Cimento 33, 906 (1964), Appendix B.
[32] The absorption parameters are defined in Ref. 13.
[33] The predicted curve is taken from M. Olsson, University of Maryland Technical Report No. 379, 1964 (unpublished).

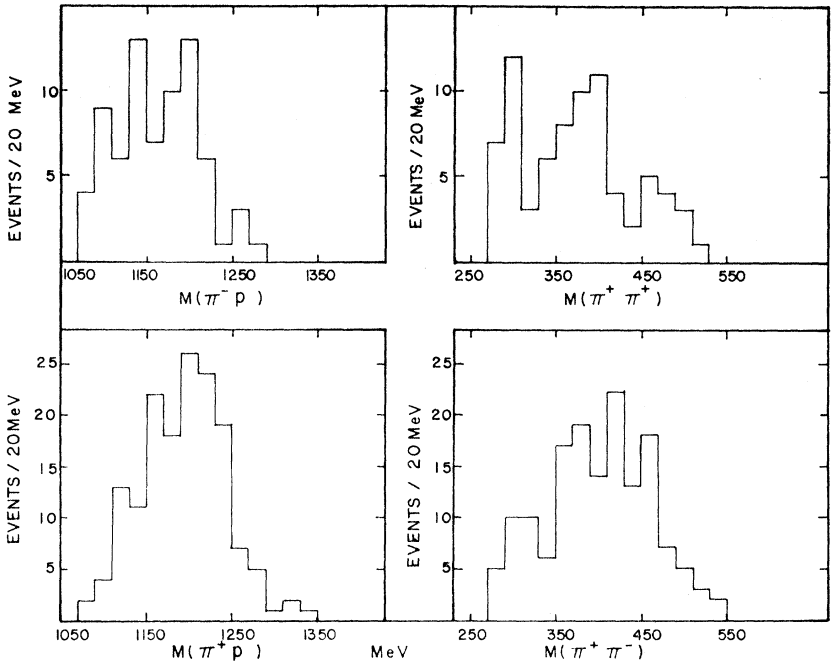

FIG. 14. Two-body mass spectra for the $\pi^+p\pi^+\pi^-$ final state.

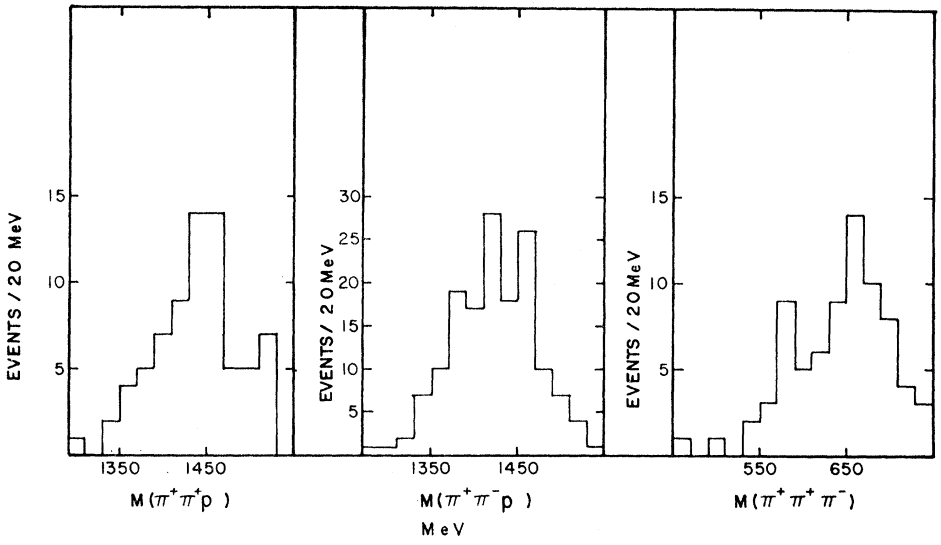

FIG. 15. Three-body mass spectra for the $\pi^+p\pi^+\pi^-$ final state.

variance also predicts

$$\frac{\sigma(N^{*+}\rightarrow\pi^0p)}{\sigma(N^{*+}\rightarrow\pi^+n)}=2. \tag{4}$$

Using this with the result (3) gives a value of 1.23 $\pm$0.13 mb for $\sigma(\pi^+p\rightarrow\pi^+N^{*+}\rightarrow\pi^+\pi^+n)$, or (66$\pm$10)% of the $\pi^+\pi^+n$ final state, which is in fairly good agreement with (1).

As mentioned in Sec. IV, the Yodh-Olsson model, which includes isospin invariance, predicts a ratio of $\sigma(\pi^+p\rightarrow\pi^+p\pi^0)/\sigma(\pi^+p\rightarrow\pi^+\pi^+n)$ of 5 which agrees with the experimental value of 4.8$\pm$0.5.

No dipion resonance with isospin $T=2$ has ever been reported, which is in agreement with these data.

We have also unambiguously identified 78 four-pronged events as follows (excluding Dalitz pairs):

$\pi^+p\rightarrow\pi^+p\pi^+\pi^-$, 76 events
$\pi^+p\rightarrow\pi^+\pi^+\pi^+\pi^-n$, 1 event
$\pi^+p\rightarrow\pi^+p\pi^+\pi^-\pi^0$, 1 event

indicating that triple pion production is highly suppressed at this energy.

For reference purposes we include in Figs. 14 and 15 the two-body and three-body invariant-mass spectra for

these 76 events. With the creation of two pions there remain only 322 MeV for the kinetic energy in the c.m. system, which is too low for appreciable N^* production.

ACKNOWLEDGMENTS

It is a pleasure to thank Dr. Ralph Shutt, Dr. K. Green, and the staffs of the AGS and of the 20-in. bubble chamber for making this exposure possible. We are particularly indebted to Dr. E. Hart who obtained the present exposure for us and suggested this problem. Professor J. D. Jackson kindly performed the absorptive-model calculations for us. We also wish to thank Dr. G. London and Dr. T. Ferbel for many helpful discussions and suggestions during the course of this experiment. Finally, we wish to acknowledge the skillful work of our scanners and measurers, Mrs. V. Miller, Mrs. L. Upelincis, and Mrs. A. Vilks, who participated in this experiment.

APPENDIX: MASS-HISTOGRAM FITTING BY THE MAXIMUM-LIKELIHOOD METHOD

The three mass histograms shown in Figs. 6(a) and 6(b) were fitted simultaneously with the quasi-two-body final states and with pure phase space using the maximum-likelihood method.[20] Assuming that the number of events in a given bin is distributed normally (Gaussian), the likelihood function may be written as

$$\mathfrak{L}(\alpha_j)=\prod_{i=1}^{N}\exp\left[-\frac{[y_i^f(\alpha_j)-y_i]^2}{2y_i}\right],$$

where N is the total number of bins in the mass histograms, y_i is the experimental value for the ith bin, and y_i^f is the fitted value.

Fitted values for the y_i^f are obtained in the following manner. A Monte Carlo program[34] generated the π^+p, π^0p, and $\pi^+\pi^0$ invariant-mass spectra for 30 000 random events for the following cases: (1) Lorentz-invariant phase space, (2) Lorentz-invariant phase space weighted by a Breit-Wigner shape for the $N^{*++}(1236)$, (3) Lorentz-invariant phase space weighted by a Breit-Wigner shape for the $N^{*+}(1236)$, (4) Lorentz-invariant phase space weighted by a Breit-Wigner shape for the $N^{*+}(1518)$, and (5) Lorentz-invariant phase space weighted by a Breit-Wigner shape for the ρ.

Then,

$$y_i^f(\alpha_1,\alpha_2,\cdots\alpha_5)=\sum_{j=1}^{5}\alpha_j y_{ij},$$

where y_{ij} is the number of events in the ith bin of the Monte Carlo output for resonance j. The α_i are subject to the constraint of normalization

$$\sum_{i=1}^{5}\alpha_i=1.$$

There are thus four free parameters.

The best estimate of the value of these parameters is obtained by maximizing $\mathfrak{L}$, or, equivalently, by minimizing

$$\chi^2=-2\ln\mathfrak{L}(\alpha_i)=\sum_{i=1}^{N}\left\{\frac{[y_i^f(\alpha_i)-y_i]^2}{y_i}\right\}$$

with respect to the α_j.

Curves of χ^2 versus α_j are shown in Fig. 16. In each case, one of the α_j is varied while the ratios of all of the other α_j, $\alpha_a:\alpha_b:\alpha_c:\alpha_d$, are held constant at their optimum values.

Since there are 70 bins in the histograms of the invariant masses, i.e., $N=70$, and since there are four free parameters, there are 66 degrees of freedom for the fit. The best fit, however, has a χ^2 of 209. Nevertheless, as seen in Fig. 16, the fit is affected strongly by small changes in the α_j for the N^{*+}'s.

To obtain confidence limits for the α_i use is made of the fact that $I_i=-2\ln\lambda_i$ is distributed for large N as χ^2 with n degrees of freedom,[21] where

$$\lambda_i=\mathfrak{L}(\alpha_1^*,\alpha_2^*,\cdots\alpha_i,\cdots\alpha_k^*)/\mathfrak{L}(\alpha_1^*,\alpha_2^*,\cdots\alpha_i^*,\cdots\alpha_k^*).$$

Where α_i^* is the value of α_i for which $\mathfrak{L}$ is a maximum and k is the number of free parameters fitted. Thus,

$$I_i=\sum_{j=1}^{N}\left\{\frac{[y_j^f(\alpha_1^*,\cdots\alpha_i^*,\cdots\alpha_k^*)-y_j]^2}{y_j}-\frac{[y_j^f(\alpha_1^*,\cdots\alpha_i,\cdots\alpha_k^*)-y_j]^2}{y_j}\right\}. \quad \text{(A1)}$$

Then, for example, the 95% confidence level on α_i is that value of α_i which makes I_i [in the above Eq. (A1)] equal to the 95% probable value of χ^2 for k degrees of freedom.

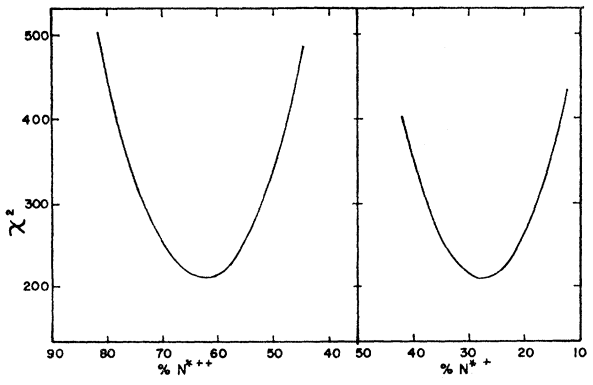

FIG. 16. χ^2 versus α for the parameters in the fitting of the mass spectra for the $\pi^+p\pi^0$ final state for the N^{*++} and N^{*+}.

[34] D. Stonehill, H. Kraybill, and J. Sandweiss, Yale University Physics Department internal report, as adapted by A. Firestone (unpublished).